PHYSICAL REVIEW D VOLUME 18, NUMBER 3 1 AUGUST 1978

Applications of interior dispersion relations to pion photoproduction near threshold

Robert McClaskey and Richard J. Jacob
Arizona State University, Tempe, Arizona 85281

Gerald E. Hite
Universität Kaiserslautern, Kaiserslautern, West Germany
(Received 13 July 1977; revised manuscript received 1 May 1978)

Interior dispersion relations are applied in the boundary limit to the determination of certain threshold and subthreshold quantities for pion photoproduction, viz., the threshold s-wave multipole amplitudes E^I_{0+}, and the amplitudes involved in the current-algebra theorems of Fubini and Furlan, and of Adler and others. Where comparisons are possible, our results are consistent with determinations by other methods. We also find further substantiation for conclusions reached elsewhere concerning the continuation of soft-pion theorems to their on-shell versions.

I. INTRODUCTION

The effectiveness of interior dispersion relations (IDR)[1] in examining the near-threshold and subthreshold behavior of pion-nucleon scattering amplitudes has been demonstrated recently in several applications. In particular, IDR have been used to obtain values of low-energy scattering parameters[2] and the pion-nucleon coupling constant[3] and σ term,[2,4] and to investigate the t dependence of subthreshold amplitudes for information regarding t-channel resonance contributions[5,6] and the validity of PCAC (partial conservation of axial-vector current) results.[7]

In addition to elastic reactions, IDR are also applicable to semielastic reactions, i.e., those of the form $a+b\to c+d$, $m_b=m_d$, and $m_a\neq m_c$, as long as the amplitudes for which the dispersion relations are written are symmetric in the kinematic variable $\nu=s-u$. In this paper we apply IDR on the boundary limit of the pion photoproduction physical region, where they have been called boundary dispersion relations (BDR),[8] to evaluate the threshold values of the E_{0+} multipoles and to examine certain current-algebra theorems, to wit, the Breit-threshold sum rules of Fubini and Furlan,[9] and the PCAC theorems of Adler[10] and others.[11]

The multipoles and Breit-threshold sum rules are obtainable directly by the on-shell procedures of IDR, and represent no difficulties in interpretation; our results are consistent with other determinations. As we shall see, however, the PCAC theorems are expressed for zero-mass pions, and their substantiation through IDR is subject to the selection of a procedure for extrapolating the mass to its physical value, which extrapolation if performed correctly should, according to PCAC, result in small variations. If, as has recently been argued by Hite, Jacob, and Scadron[7] for elastic pion-nucleon scattering, the proper procedure is to fix the variables ν and t, as opposed to ν and ν_B, the on-shell versions of the PCAC theorems are unfortunately not within the reach of evaluation by IDR. On the other hand, the point in the space of kinematical variables which is reached by fixing ν and ν_B and bringing the pion mass to its physical value *is* accessible to IDR, and our analysis is performed at this point. In pion-nucleon scattering, this is the point at which, for the appropriate amplitude, the on-shell πN σ term is calculated, the value of which is by now generally agreed to be large by PCAC variational standards.[12] However, as argued by HJS, since this is not the proper quantity to which to refer the off-shell pion-nucleon PCAC theorem,[13] no inconsistency between PCAC and a large σ term is seen.

We find a similar circumstance for pion photoproduction. Evaluations of the amplitudes in the PCAC theorems by others, using fixed-t dispersion-relation methods at what we would call the proper on-shell point, yield results which vary only slightly (10–15%) from the predicted off-shell values. However, our determinations of the amplitudes at the "improper" point results in larger variations (~50%) resembling those in the analogous pion-nucleon situation.

II. INTERIOR DISPERSION RELATIONS FOR PION PHOTOPRODUCTION

The advantages of IDR, relative to other dispersion-theoretic techniques, have been discussed previously in detail,[14] and we only summarize them here: 1. The s-channel integrals converge rapidly for the amplitudes considered, and there is no need for subtractions of high-energy parametrizations. 2. The s-channel contributions are evaluated at intermediate laboratory-frame angles and

represent generally a more reliable application of original scattering data in the multipole determinations; effects of final state Coulomb interactions are also thereby reduced. 3. The smoothness of the discrepancy function permits a relatively credible extrapolation to near-threshold and subthreshold points. 4. In certain types of calculations, such as those presented here, the effects of truncation errors in the s-channel integral are significantly reduced by their own smoothness as a function of t at small t values, and are further offset in the process of recovering the amplitude at the extrapolation point. Typically, integration errors, due to truncation at high energies, of 10% or so yield uncertainties of less than 1% in the final result. A significant disadvantage of IDR for semielastic processes is the inaccessibility of most of the near subthreshold region (real ν and t) to direct analysis.

A detailed discussion of IDR for semielastic reactions is given in the Appendix. The IDR for pion photoproduction amplitudes has the form

$$\mathrm{Re}\tilde{A}(t,a)=\tilde{A}^{B}_{\mathrm{IDR}}(t,a)+\frac{1}{\pi}\mathrm{P}\int_{\bar{s}}^{-\infty}\frac{\mathrm{Im}\tilde{A}^{s}(t',a)}{t'-t}dt'+\frac{1}{\pi}\mathrm{P}\int_{\bar{t}}^{0}\frac{\mathrm{Im}\tilde{A}^{s}(t',a)}{t'-t}dt'+\Delta_{s}(t,a)+\frac{1}{\pi}\mathrm{P}\int_{t_2}^{\infty}\frac{\mathrm{Im}\tilde{A}^{t}(t',a)}{t'-t}dt', \quad (2.1)$$

where $\tilde{A}$ is an invariant amplitude which is symmetric, or has been symmetrized, in ν,

$$\tilde{A}=\begin{cases}A\\ A/\nu\end{cases}\ \text{if}\ A(\nu,t)=\begin{cases}+A(-\nu,t)\\ -A(-\nu,t)\end{cases}. \quad (2.2)$$

$\tilde{A}^{B}_{\mathrm{IDR}}$ is the gauge-invariant Born-term contribution, $t_2=4\mu^2$, μ being the pion mass, and Δ_s and $\bar{t}$ are defined for general a in the Appendix.

As we shall see in Sec. III, our interest in this paper is in IDR with the path parameter $a=0$, where the integration path includes the entire s-channel physical-region boundary and the $\theta_t=\pi$ portion of the t-channel physical-region boundary, in addition to the nonphysical segment extending from $t=t_2$ to $t=4m_N{}^2$. In this case we have $\Delta_s=0$, $\bar{s}=s_2=(\mu+m_N)^2$, and $\bar{t}=-\mu^2(1-\mu/m_N)$. Identifying the t-channel integral as the discrepancy function $D(t,a)$, and introducing a self-explanatory notation for the s-channel integrals, we have for $a=0$,

$$D(t,0)=\mathrm{Re}\tilde{A}(t,0)-\tilde{A}^{B}_{\mathrm{IDR}}(t,0)-I^{-}_{s}(t,0)-I^{+}_{s}(t,0). \quad (2.3)$$

III. THE CURRENT-ALGEBRA THEOREMS

The current-algebra commutation relation

$$[Q^{i}_{A},V^{3}_{\mu}(0)]=i\epsilon_{i3k}A^{k}_{\mu}(0), \quad (3.1)$$

where $V^{i}_{\mu}(x)$ and $A^{i}_{\mu}(x)$ are the vector and axial-vector hadronic current operators, and

$$Q^{i}_{A}=\int d^3r\,A^{i}_{0}(x),$$

has been reduced to sum rules for pion photoproduction by various techniques. Invoking the PCAC hypothesis,

$$\partial_{\mu}A^{i}_{\mu}(x)=[\sqrt{2}\,\mu^2 m_N g_A(0)/g_{\pi}(0)]\phi^{i}_{\pi}(x), \quad (3.2)$$

several authors[10,11] have deduced soft-pion relations for electroproduction amplitudes, of which the following survive in the photoproduction limit:

$$\bar{A}^{+}_{1}(\nu=0,\nu_B=0;\ q^2=0)=(e_{\pi}g_{\pi}(0)/2m_N)F^{V}_{2}(0), \quad (3.3a)$$

$$\bar{A}^{0}_{1}(\nu=0,\nu_B=0;\ q^2=0)=(e_{\pi}g_{\pi}(0)/2m_N)F^{S}_{2}(0), \quad (3.3b)$$

where $F^{V}_{2}(k^2)$ and $F^{S}_{2}(k^2)$ are the isovector and isoscalar nucleon Pauli form factors, respectively, as functions of the photon invariant mass^2 k^2 with normalization $F^{V}_{2}(0)=3.70/2m_N$ and $F^{S}_{2}(0)=-0.12/2m_N$; q^2 is the pion invariant mass^2, $\nu=s-u$ and $\nu_B=t-q^2$. $\bar{A}^{+,0}_{1}$ are the non-Born real parts of the Chew-Goldberger-Low-Nambu (CGLN) invariant amplitudes[15] (we use the notation of Ball[16]). Finally, $e_{\pi}{}^2/4\pi=1/137$, $g_{\pi}(q^2)$ is the pion-nucleon coupling form factor with $g_{\pi}{}^2(\mu^2)/4\pi\simeq 14.7$, and $g_A(0)=1.25$. Under the assumption $g_{\pi}(0)\simeq g_{\pi}(\mu^2)$, the PCAC theorems, Eqs. (3.3), become

$$\bar{A}^{+}_{1}(0,0;0)=0.083\,3\mu^{-2}, \quad (3.4a)$$

$$\bar{A}^{0}_{1}(0,0;0)=-0.002\,73\mu^{-2}. \quad (3.4b)$$

The IDR evaluations of these amplitudes will be for physical photoproduction, i.e., on-shell pions; consequently, comparison with the PCAC predictions will require accounting for the method by which the on-shell versions of Eqs. (3.4) are written. The two commonly used nonequivalent methods[17] involve holding ν at the symmetry point $\nu=0$, and bringing q^2 from 0 to μ^2 by varying either ν_B or t, respectively. In a discussion of this problem as it relates to pion-nucleon scattering, HJS argue from IDR and other results that, of the two alternatives, fixing t and allowing ν_B to vary is to be preferred, inasmuch as it results in a variation of only 10–15% of the PCAC predictions, whereas the variations encountered by fixing ν_B and allowing t to vary are significantly greater.

The values of the pertinent photoproduction vari-

ables are as follows:

	ν	ν_B	t	q^2	a
Off-shell	0	0	0	0	m_N^2
(I) On-shell, fixed t	0	$-\mu^2$	0	μ^2	$+\infty$
(II) On-shell, fixed ν_B	0	0	μ^2	μ^2	0 .

We see that only case II is amenable to IDR techniques, a having to be ≤ 0 in order for the integration paths to be contained within the physical regions. Our calculation will be carried out at this point, which is analogous to the σ-term point[18] of pion-nucleon scattering. Our results will be used in connection with estimates by other authors of the amplitudes at point I to compare the relative variations of the PCAC amplitudes under the two alternative continuation schemes.

Questions of extrapolation in the pion mass do not occur in evaluating the relationships derived by Fubini and Furlan,[9] who started from the commutator, Eq. (3.1), saturated the one-nucleon matrix elements with a complete set of intermediate states, and evaluated them in the Breit frame, keeping the pion on the mass shell. At the Breit threshold, given by $\vec{P}_1 + \vec{P}_2 = 0$, $\vec{q} = 0$, the following sum rules were obtained:

$$T_1^+(\mathrm{BT}) = (\mu/4f_\pi E)G_E^V(t)g_A(0) + d_1^+ , \tag{3.5a}$$

$$T_1^0(\mathrm{BT}) = (\mu/4f_\pi E)G_E^S(t)g_A(0) + d_1^- , \tag{3.5b}$$

$$T_1^-(\mathrm{BT}) = (-1/2f_\pi)[g_A(t) + (t/4E^2)G_M^V(t)g_A(0)] + d_1^- , \tag{3.5c}$$

where, in terms of the CGLN amplitudes,

$$e_\pi T_1^i = -(m_N\mu/E)A_1^{(i)} - \mu^2 A_3^{(i)} + (\mu t/2E)A_4^{(i)} , \tag{3.6}$$

$E = (m_N^2 - t/4)^{1/2}$, $G_{M,E}^{v,s}$ are the Sachs electromagnetic form factors, and the d_1^i are correction integrals. f_π and $g_\pi(0)$ are related through the Goldberger-Treiman relation, $f_\pi = m_N g_A(0)/g_\pi(0)$.

The Breit threshold corresponds to the point $t = -\mu^2$, $a = 0$ [$\nu = 2\mu(4m_N^2 - \mu^2)^{1/2}$, $\nu_B = 0$] and is therefore accessible to evaluation by the boundary version of IDR.

IV. EVALUATION OF THE DISPERSION RELATIONS

Our technique in general is to evaluate the discrepancy function for physical values of t from Eq. (2.3), using the (pseudoscalar) Born terms and s-channel multipoles as fitted to photoproduction data. The discrepancy function is then extrapolated, using a polynomial fitting function, to the desired point t_θ, at which the real part of the amplitude is recovered using Eq. (2.3) in the form [in evaluating $\bar{A}$ for the PCAC theorem, the ordinary fixed-t dispersion-relation Born term A_N is subtracted from the right-hand side of Eq. (4.1).]

$$\mathrm{Re}\bar{A}(t_\theta, a) = D(t_\theta, a) + \bar{A}_{\mathrm{IDR}}^B(t_\theta, a) + I_s^-(t_\theta, a) + I_s^+(t_\theta, a) . \tag{4.1}$$

To evaluate the s-channel integrals and real parts of the amplitudes at physical t values, we use the multipole analysis of Moorhouse, Oberlack, and Rosenfeld,[19] supplemented at low energies within the integrals by the imaginary parts of the multipoles of Berends, Donnachie, and Weaver.[20] The MOR analysis used a K-matrix technique to parametrize resonance and background contributions to the imaginary parts of the amplitudes. The real parts were then calculated from fixed-t dispersion relations. This resulted in relatively smooth real parts and smooth discrepancy functions in the photon energy range (270–1200 MeV) of the analysis. Real parts obtained from the BDW multipoles at low energies yielded variations in the discrepancy functions which contributed nothing to our confidence in the extrapolations, and were therefore not included in the analysis. Moreover, since multipole fits are least reliable at far-forward angles, the discrepancy functions calculated at very small negative values of t, in the region where the contributions are primarily evaluated at $\theta_s = 0$, are also not reliable constraints on the extrapolations. We therefore have included only those values of $D(t, 0)$ for $t \leq -0.16$ GeV^2, corresponding to $\theta_s = \pi$ and $E_\gamma > 270$ MeV. The range of t values used was taken to be as large as possible while still requiring only a quadratic parametrization of $D(t, 0)$ for a best fit.

The Born terms are calculated from the usual gauge-invariant pseudoscalar-pole diagrams. In general, for fixed physical a, there are two images of the nucleon poles in the complex t plane. At $a = 0$, however, they coincide at $t_N = \mu^2$. Their contributions to the Cauchy integral formula result in the following:

$$\begin{aligned}
&(\bar{A}_1^{+,0})_{\mathrm{IDR}}^B = -\eta I_1(t) , \quad (\bar{A}_1^-)_{\mathrm{IDR}}^B = -\eta I_2(t) , \\
&(\bar{A}_2^{+,0})_{\mathrm{IDR}}^B = 2\eta I_2(t) , \quad (\bar{A}_2^-)_{\mathrm{IDR}}^B = 2\eta I_3(t) , \\
&(\bar{A}_3^{+,0})_{\mathrm{IDR}}^B = (\eta/2m_N)(\mu_p \mp \mu_N)I_2(t) , \\
&(\bar{A}_3^-)_{\mathrm{IDR}}^B = (\eta/2m_N)(\mu_p - \mu_N)I_1(t) , \\
&(\bar{A}_4^{+,0})_{\mathrm{IDR}}^B = (\eta/2m_N)(\mu_p \mp \mu_N)I_1(t) , \\
&(\bar{A}_4^-)_{\mathrm{IDR}}^B = (\eta/2m_N)(\mu_p - \mu_N)I_2(t) ,
\end{aligned} \tag{4.2}$$

where

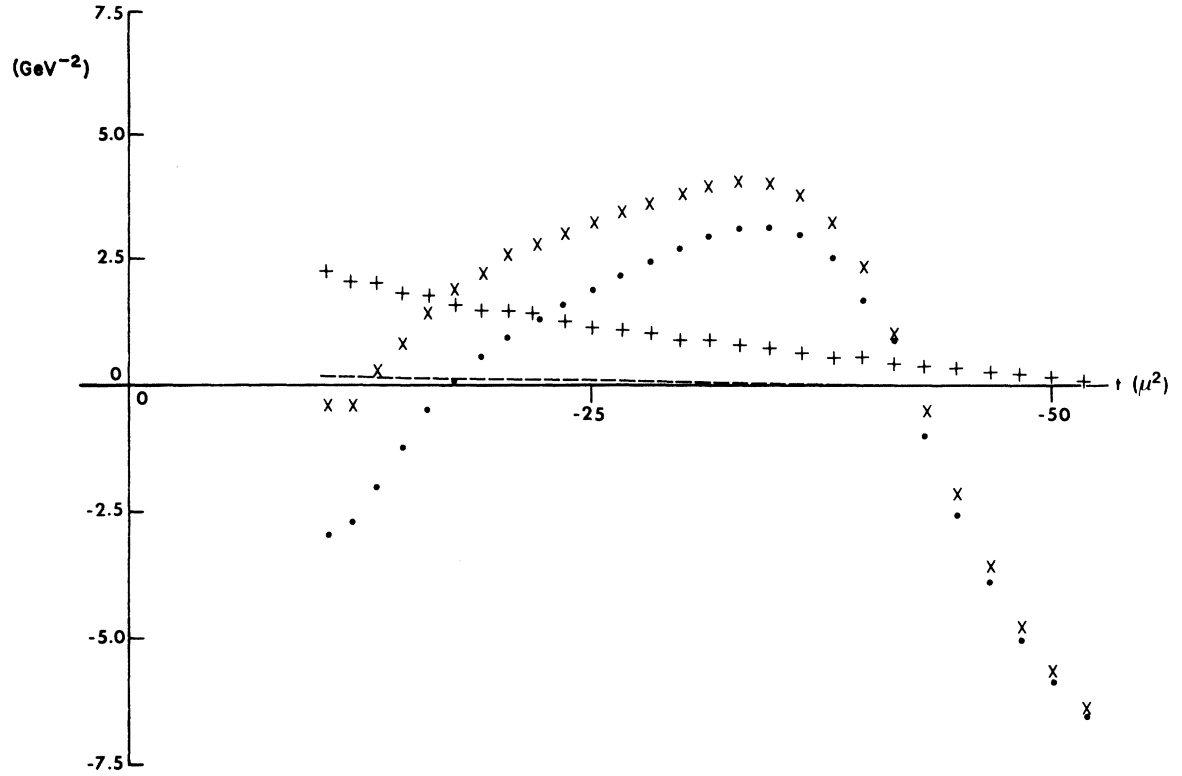

FIG. 1. s-channel physical-region contributions and discrepancy function for A_1^+. Dashed line indicates combined A_{IDR}^B and I_s^+, dotted line indicates I_s^-, xxx indicates ReA_1^+, +++ indicates $D(t,0)$.

$$I_1(t) = \frac{\mu^2}{m_N^2(t-\mu^2)},$$

$$I_2(t) = \frac{t}{m_N^2(t-\mu^2)^2},$$

$$I_3(t) = \frac{t}{m_N^2(t-\mu^2)^3},$$

$\eta = e_r g_r/2$, $\mu_p = 1.79$, and $\mu_N = -1.91$.

The contributions to the discrepancy function from the integrals, Born term, and real part are shown for the typical case of A_1^+ in Fig. 1. The integrals were performed using a data-point integration routine which requires knowledge of the imaginary parts only at energies for which they are provided in the multipole analysis. Integration is truncated at the end of the MOR energy range, but convergence for $I_s^-(t,0)$ was tested by adding a high energy u-channel Regge parametrization,[21] and the truncation error estimated to be less than 10% of the integral. Since the value of the truncation loss varies slowly for small t, and is at any rate a smooth function of t, its contribution to the final error estimate is small.[22] The arguments pertinent to the case of I_s^- do not apply to I_s^+, however. The forward integral is relatively small in the range of t values for which $D(t,0)$ is calculated from the data, but is not insignificant at the extrapolation points; neither is the truncation loss slowly varying. The uncertainties given in our final results include, therefore, an estimated 20% truncation error in the forward integrals.

The nearest singularity of the discrepancy function to the region of interest in this paper is a cut beginning at the two-pion threshold, i.e., at the lower limit of the t-channel integral in Eq. 2.1. The effect of this branch point on the smoothness of the discrepancy function is believed to be small since the character of $D(t)$ is governed primarily by the much stronger resonance singularities at larger values of t. One expects that at most there is a small cusp in $D(t)$ at $t = t_2$. That this cusp is indeed small and that it introduces no severe variations in the curvature of the discrepancy function as one approaches it from $t < t_2$ can be substantiated by fitting the data with a power series in the variable $\tau \equiv (1 - t/4\mu^2)^{1/2}$, as a function of which the discrepancy function has no branch point at $t - t_2$, or by fitting the data to t-channel resonance

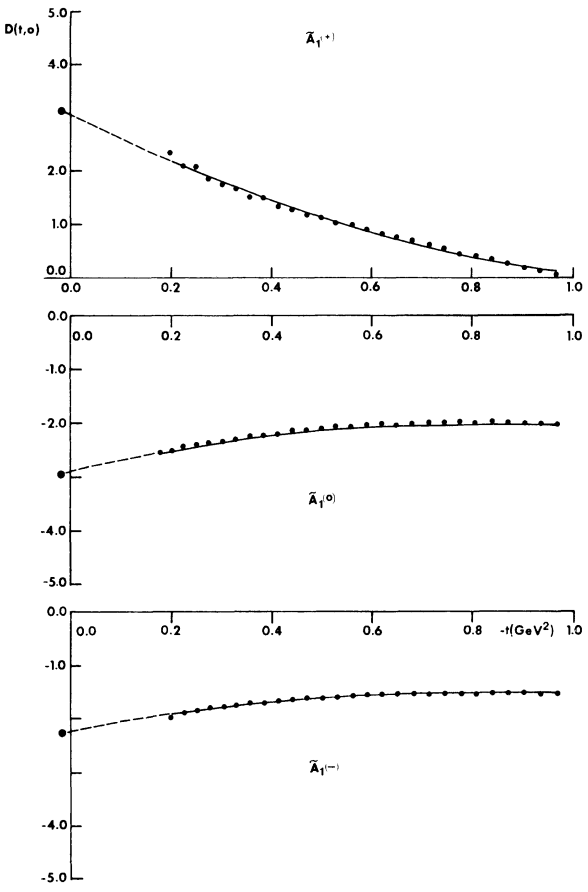

FIG. 2. Discrepancy functions for $\tilde{A}_1^I$, showing the best quadratic fit and extrapolation to $t=\mu^2$. Other extrapolations in this paper are to $t=-\mu^2$ (Breit threshold) and $t=-\mu^2(1-\mu/m_N)$ (physical threshold). $D(t,0)$ is shown in GeV units appropriate to the amplitudes (see Table I).

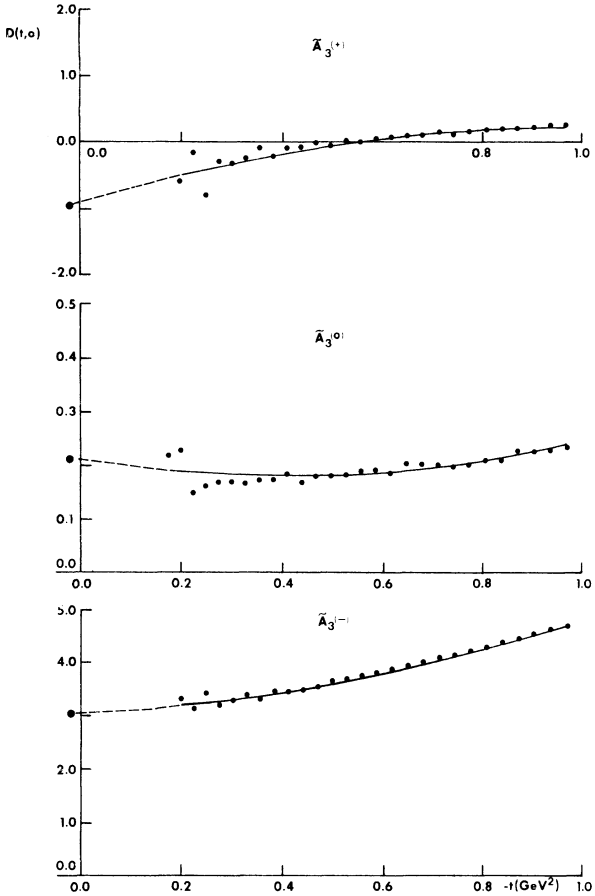

FIG. 3. Same as Fig. 2 for $\tilde{A}_3^I$. Large fluctuations near $t=-0.2$ GeV^2 in some amplitudes are due to large cancelations of imperfectly matched and rapidly varying real parts and "backward" integrals near the position of the $\Delta(1236)$ resonance.

model forms for $D(t)$ which incorporate the two-pion threshold behavior. We find that variations in the extrapolation results obtained from these methods as compared to the fits to polynomials in t are comparable to or less than the uncertainties from other sources as described below. Indeed, on the scales as given in Figs. 1–4, the cusp as calculated from $J=1$ resonance plus background models is imperceptible. In order to investigate the detailed nature of this cusp, multipole amplitudes at lower energies and of greater precision are required.

We have incorporated in our error estimates a contribution representing this variance from the smoothness assumption as estimated by comparing the results of using polynomials in t and in τ. We prefer, however, to select and display the fits to polynomials in t for the following reasons: (a) Once it has been justified to fit data to a polynomial of finite order, the reliability of the extrapolation is governed in part by the relative length of the extrapolation distance to that of the data region. The variable t has the distinct advantage here. (b) In terms of the variable t, the discrepancy function clearly displays the resonance-tail behavior one expects for all amplitudes except $A_3^{(0)}$, to which no known $J=1$ resonance couples. The discrepancy function for $A_3^{(0)}$ is due to background, higher-order singularities, and is quite flat. As can be seen from Tables I and III, the results given in this paper are insensitive to the extrapolations of the discrepancy function for this amplitude.

The discrepancy functions for all amplitudes considered are shown along with the best fits and extrapolations in Figs. 2–4. Over the range of t values shown, the discrepancy functions were all fit best by quadratic polynomials. Due to the diffi-

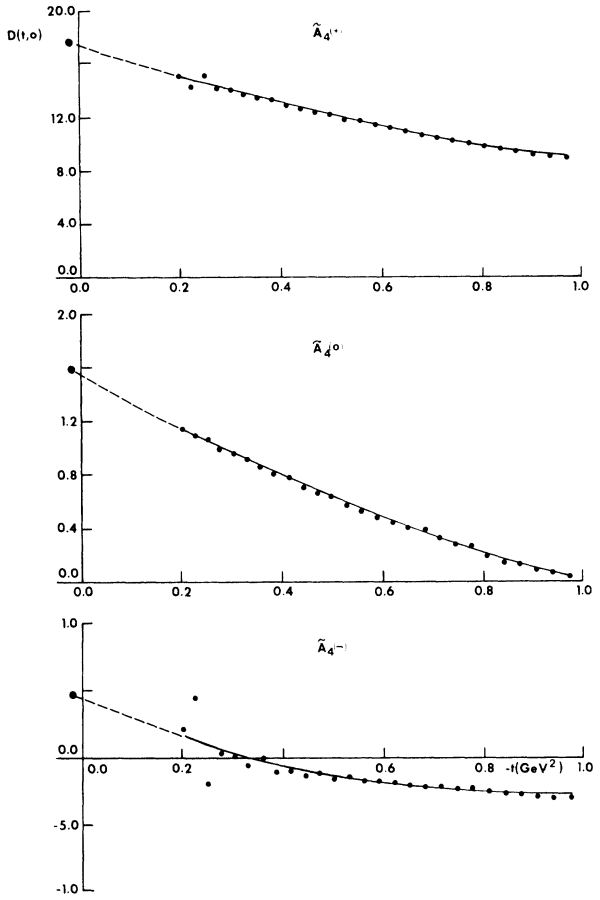

FIG. 4. Same as Figs. 2 and 3 for $\tilde{A}_4^I$.

culty of obtaining reliable data-related uncertainties in $D(t,0)$ at each value of t, all points were weighted equally. Error estimates given here include: (1) the statistical extrapolation uncertainty, as obtained from the χ^2 error matrix, (2) a 20% uncertainty in the value of I_s^+, (3) a 1% uncertainty in the value of g_r,[3] and a 1% effect on the recovered amplitude of a 10% error in I_s^-. The integral-truncation errors are believed to have been generously overestimated, but the statistical uncertainties in the extrapolation are quite small, owing to the smoothness of the discrepancy functions. As discussed earlier, this smoothness reflects the fixed-t dispersion relation constraints on the multipole analysis; our error estimates do not include any systematic errors which may exist in the multipoles.

V. RESULTS AND DISCUSSION

A. s-wave electric multipoles

At threshold, the s-wave electric multipole amplitude is related to the invariant amplitudes according to

$$\frac{8\pi(m_N+\mu)^2}{\mu(2m_N+\mu)[m_N(m_N+\mu)]^{1/2}}E_{0+}^I = A_1^I + \frac{\mu(2m_N+\mu)}{2(m_N+\mu)}A_3^I + \frac{\mu^2}{2(m_N+\mu)}A_4^I. \quad (5.1)$$

The values in Table I yield

TABLE I. Contributions and recovered real parts from Eq. (4.1) at $t = \tilde{t}$.

	D	$\tilde{A}^B_{\mathrm{IDR}}$	I_s^-	I_s^+	Total = Re $\tilde{A}$
$\tilde{A}_1^+$ (GeV^{-2})	2.99 ± 0.48	1.24	0.60	1.80	6.63 ± 0.60
$\tilde{A}_1^0$ (GeV^{-2})	-2.84 ± 0.34	1.24	-0.03	0.12	-1.51 ± 0.35
$\tilde{A}_1^-$ (GeV^{-4})	-2.20 ± 0.29	30.00	0.14	0.79	.28.73 ± 0.45
$\tilde{A}_3^+$ (GeV^{-5})	-0.86 ± 0.34	-58.81	-1.35	-15.47	-78.49 ± 3.16
$\tilde{A}_3^0$ (GeV^{-3})	0.21 ± 0.02	2.08	-0.01	-0.23	2.05 ± 0.06
$\tilde{A}_3^-$ (GeV^{-3})	3.07 ± 0.34	-2.44	0.78	7.36	8.77 ± 1.51
$\tilde{A}_4^+$ (GeV^{-3})	17.10 ± 0.68	-2.44	2.96	30.25	47.87 ± 6.09
$\tilde{A}_4^0$ (GeV^{-3})	1.50 ± 0.11	-0.09	-0.01	-0.16	1.24 ± 0.11
$\tilde{A}_4^-$ (GeV^{-5})	0.41 ± 0.30	-58.81	-1.30	-15.20	-74.90 ± 3.11

TABLE II. Charge-state threshold multipoles $E_{0+}(0)$. Units are $10^{-2}\,\mu^{-1}$

	$\gamma p \to \pi^+ n$	$\gamma n \to \pi^- p$	$\gamma p \to \pi^0 p$
Mullensienfen, *et al.* Ref. 29	...	...	0.17
Adamovich, *et al.* Ref. 30	2.83 ± 0.05	-3.18 ± 0.20	...
Nölle Ref. 31	2.98	-3.52	-0.19
Present calculation	2.75 ± 0.12	-3.27 ± 0.12	0.066 ± 0.164

$$E_{0+}^{+} = (0.25 \pm 0.16)\times 10^{-2}\mu^{-1},$$
$$E_{0+}^{0} = (-0.18 \pm 0.05)\times 10^{-2}\mu^{-1}, \qquad (5.2)$$
$$E_{0+}^{-} = (2.13 \pm 0.09)\times 10^{-2}\mu^{-1}.$$

There have been numerous evaluations of the threshold multipoles over the past two decades. Here we offer for comparison in Table II those listed in the most recent edition of the compilation of coupling constants and low-energy parameters (Nagels *et al.*[23]) for pion charge states.

B. Fubini-Furlan sum rules

The values of the various contributions to the amplitudes in Eq. (3.6) at the Breit threshold are given in Table III, and our results given in Table IV, along with those of Furlan, Paver, and Verzegnassi[24] and von Gehlen and Schmidt.[25] FPV evaluated the sum rules, Eqs. (3.5), by assuming reasonable dipole models for the electromagnetic form factors and estimating the correction integrals using threshold behavior, N^* isobaric models, and vector-meson contributions. They then predicted values of the amplitudes and computed Breit-threshold differential cross sections which were in reasonable agreement with the nearly physical threshold cross sections for charged-pion photoproduction.

Rather than evaluate the correction integrals, GS determined the amplitude $T_1^{(-)}$ at the Breit threshold directly with fixed-t dispersion relations, using as input s- and p-wave multipoles as given by von Gehlen,[26] and a resonance model for d-wave multipoles. Their result allowed a prediction of the correction term, d_1^-, which is consistent with our prediction, although significantly less than that calculated explicitly by FPV. The variations in the respective values of T_1^-, can be accounted for entirely by those in the values of d_1^-.

Our values of T_1^0 and d_1^0 are consistent with those of FPV, and the uncertainties in our values of T_1^+ and d_1^+ do not preclude agreement there as well. The experimental situation, however, is still not adequately known to be able to compare predictions for the threshold cross sections for π^0 production.

TABLE III. Contributions and recovered real parts from Eq. (4.1) at $t = t_{BT} = -\mu^2$.

	D	$\tilde{A}^B_{IDR}$	I_s^-	I_s^+	Total = Re $\tilde{A}$
$\tilde{A}_1^+$ (GeV^{-2})	2.98 ± 0.48	1.16	0.49	1.94	6.58 ± 0.60
$\tilde{A}_1^0$ (GeV^{-2})	-2.83 ± 0.34	1.16	-0.02	0.12	-1.57 ± 0.35
$\tilde{A}_1^-$ (GeV^{-4})	-2.20 ± 0.29	30.14	0.10	0.87	28.90 ± 0.45
$\tilde{A}_3^+$ (GeV^{-5})	-1.00 ± 0.34	-59.09	-1.17	-15.76	-77.02 ± 3.16
$\tilde{A}_3^0$ (GeV^{-5})	-0.21 ± 0.02	2.09	-0.01	-0.24	2.05 ± 0.06
$\tilde{A}_3^-$ (GeV^{-3})	3.08 ± 0.34	-2.28	0.66	7.53	8.99 ± 1.51
$\tilde{A}_4^+$ (GeV^{-3})	17.07 ± 0.68	-2.28	2.53	30.85	48.17 ± 6.09
$\tilde{A}_4^0$ (GeV^{-3})	1.50 ± 0.11	0.08	0.01	-0.16	1.42 ± 0.11
$\tilde{A}_4^-$ (GeV^{-5})	0.41 ± 0.30	-59.09	-1.12	-15.49	-75.30 ± 3.11

TABLE IV. Values for the Fubini-Furlan sum-rule amplitudes and predicted values for the correction terms. Units are μ^{-1}

	T_1^+	d_1^+	T_1^0	d_1^0	T_1^-	d_1^-
FPV	0.010	-0.019	0.081	0.056	-1.20	-0.26
GS	...	...	...	...	-1.05	-0.09
Present calculation	-0.093 ± 0.206	-0.160 ± 0.206	0.090 ± 0.060	0.063 ± 0.060	-1.02 ± 0.12	-0.056 ± 0.11

C. The PCAC theorems

Quantities relevant to the determination of $\bar{A}_1^{+,0}$ at the point indicated as case II in Sec. III are given in Table V. $\bar{A}_1^{(+)}$ at the case-I point has been calculated by Adler and Gilman[27] and by von Gehlen and Schmidt,[25] while both $\bar{A}_1^{(+)}$ and $\bar{A}_1^{(-)}$ at the same point were calculated by Gensini *et al.*,[28] all using various fixed-t dispersion-relation approaches. Their results (see Table VI) are all consistent with small variations from the soft-pion predictions. The IDR determinations at the case-I point, on the other hand, are of somewhat greater variation from the off-shell values, although the smallness of $\bar{A}_1^{(0)}$ along with the relatively large uncertainty discourages the drawing of any firm conclusions regarding it. Nevertheless, the indicated trend of variations, i.e., greater and in the opposite direction for case II than for case I, is consistent with that found by HJS for pion-nucleon scattering, and supports their conclusion regarding the proper prescription for continuing PCAC theorems from the soft-pion to the on-shell point.

ACKNOWLEDGMENT

We wish to acknowledge helpful communications from Dr. E. Borie.

APPENDIX: INTERIOR DISPERSION RELATIONS FOR SEMIELASTIC REACTIONS

We categorize as semielastic any reaction of the type

$$a+b\to c+d\,, \tag{A1}$$

where the mass of one of the initial particles equals that of one of the final particles. For definiteness, we take $m_b = m_d \equiv m$, $m_a \neq m_c$, refer to (A1) as the s-channel process and adopt the conventional Mandelstam variables $s=(p_a+p_b)^2$, $t=(p_a-p_c)^2$, and $u=(p_a-p_d)^2$ with their interrelationship $s+t+u=2m^2+m_a^2+m_c^2\equiv\Sigma$. We also define the invariant $\nu\equiv s-u$, and introduce the Kibble boundary function, which vanishes along the boundaries of the physical region of process (A1) and its crossing-associated reactions,

$$\phi(\nu,t)=4t(p_tp_t'\sin\theta_t)^2=4s(p_sp_s'\sin\theta_s)^2\,. \tag{A2}$$

Here, p, p', and θ are the initial and final three-momenta and scattering angle in the center-of-mass system of the indicated reaction channel. We have, in particular,

$$4p_tp_t'=\frac{1}{t}\{t(t-4m^2)[t-(m_a+m_c)^2][t-(m_a-m_c)^2]\}^{1/2}$$

$$\equiv -\nu_t \tag{A3}$$

and

$$\cos\theta_t=-\nu/\nu_t\,. \tag{A4}$$

For elastic and semielastic processes, the s and u channels are kinematically equivalent, and the invariant amplitudes are either symmetric or antisymmetric in ν. As a function of ν and t, an invariant amplitude presumably has only dynamica singularities, but if one fixes a variable which is itself a nonanalytic function of ν and t, spurious "kinematical" singularities are introduced which must be included in any dispersion relation writen in the remaining free variable. The discontinuity

TABLE V. Contributions and recovered real parts at $t=\mu^2$ for the PCAC-theorem amplitudes. $\tilde{A}_N$ is the usual fixed-t dispersion-relation Born term.

	D	I_s^-	I_s^+	$\tilde{A}^B_{\rm IDR}-\tilde{A}_N$	Total = Re $\tilde{\bar{A}}$
$\tilde{A}_1^+$ (GeV^{-2})	3.16 ± 0.48	-0.33	1.07	2.33	(6.23 ± 0.526)
$\tilde{A}_1^0$ (GeV^{-2})	-2.92 ± 0.34	0.13	0.14	2.33	(-0.43 ± 0.34)

TABLE VI. PCAC-theorem amplitudes as predicted and calculated in cases I and II.

	$\bar{A}_1^+$	$\bar{A}_1^0$
Theoretical (off shell)	$0.083\ 3\mu^{-2}$	$-0.002\ 73\mu^{-2}$
Calculated (on shell, case I)		
AG	0.071 5	...
GS	0.080 0	...
GKPV	0.079 7 ± 0.029 9	0.000 32 ± 0.000 34
Present calculation (on shell, case II)	0.120 ± 0.010	−0.008 3 ± 0.006 6

or residue of the amplitude at this singularity being generally unknown and unobtainable from the dynamics of the interaction, the dispersion relation so obtained has little value. For amplitudes symmetric in ν, however, a variable which *can* be fixed to obtain kinematical-singularity-free dispersion relations is the path parameter

$$a \equiv -\phi(\nu, t)/t^2 , \tag{A5}$$

as can be seen from the relationship

$$\nu^2 = \nu_t^2 + 4at . \tag{A6}$$

Interior dispersion relations (IDR) are written for ν-symmetric amplitudes (antisymmetric amplitudes can be symmetrized by dividing by ν) by fixing a and writing the Cauchy integral formula for the amplitude in the complex t plane.

From (A6), we see that the mapping $\nu(t, a)$ requires a two-sheeted t plane. On the sheet for which $\nu = +(\nu_t^2 + 4at)^{1/2}$, we have

$$2s(t, a) = \Sigma - t + (\nu_t^2 + 4at)^{1/2} , \tag{A7a}$$

$$2u(t, a) = \Sigma - t - (\nu_t^2 + 4at)^{1/2} . \tag{A7b}$$

It is this sheet upon which are found the images of the s-channel singularities, while the u-channel singularities are mapped onto the second sheet. The t-channel singularities are found, of course, on both sheets.

To examine the mapping of the s-channel singularities we find the roots of the quadratic equation for t which is obtained from Eq. (A7a):

$$t_\pm(s, a) = \frac{-b \pm [b^2 - 4c(s-a)]^{1/2}}{2(s-a)} , \tag{A8}$$

where

$$b = [(4sp_a p_a')^2 + 4sc]^{1/2} ,$$

$$c = m^2(m_a^2 - m_c^2)^2 .$$

In general, s-channel singularities will have two images. Fixing a at a value ≤ 0 results in the image of the s-channel unitarity cut being a path which lies for the most part within the s-channel phys-

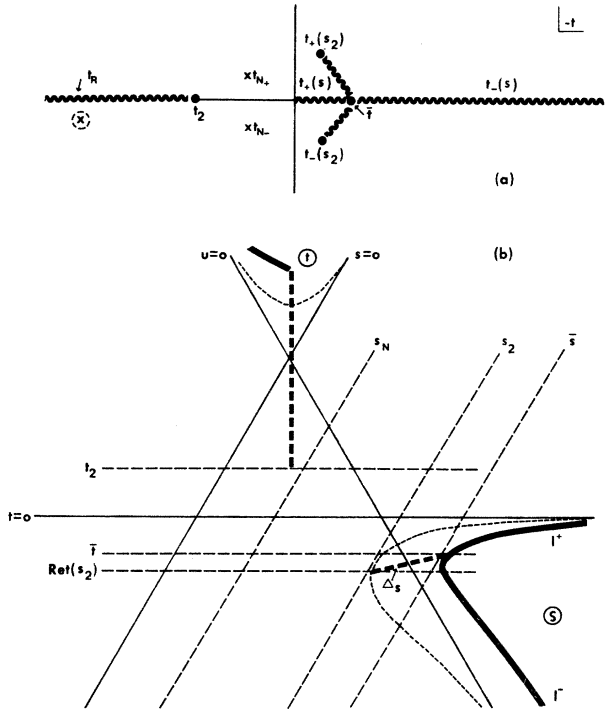

FIG. 5. Schematic representation of dynamical singularities for semielastic reactions. (a) shows the t channel, and images of the s channel, cuts and poles in the complex-t plane for fixed $a < 0$. The "pig tails" leave the real t axis at $\bar{t}$ and progress to $t^\pm(s_2)$ as s approaches its threshold value, s_2. For $a = 0$, $t^\pm(s_2) = \bar{t}$, and $t_{N+} = t_{N-}$ is also real. t_2 is the t-channel unitarity hadronic threshold, and t_R represents the position of a t-channel resonance on the second *dynamical t* sheet. The Mandelstam diagram (b) shows the location of these singularities with respect to the s- and t-channel physical regions. The u-channel unitarity cut appears on another *kinematical t* sheet, does not contribute to the dispersion relation, and is not pictured here. Physical-region boundaries are indicated by short-dashed lines and physical integration paths by heavy continuous lines. Heavy-dashed lines represent contributions to the dispersion relation from amplitudes at complex values of t, Δ_s being the contribution of the "pig tails" in (a). For $a = 0$, $\Delta_s = 0$, both heavy solid and dashed lines for $t > t_2$ contribute to the discrepancy function, $D(t, a)$.

ical region, as shown in Fig. 5. For nonpositive a, we let $\bar{s}(a)$ denote the value of s at the branch point in Eq. (A8). We have $\bar{s}(a) \geq s_2$, where s_2 is the two-hadron s-channel threshold, $\bar{s}(0) = s_2$. For $s \geq \bar{s}(a)$, $t_\pm(s, a)$ are real and the amplitudes evaluated along these portions of the path (heavy-dashed line in Fig. 5) are physical. t_+ corresponds generally to forward, and t_- to backward, scattering angles, although $\cos\theta_s(\bar{s}, a) = 0$ only for $a = 0$. In the range $s_2 \leq s < \bar{s}$, $t_\pm$ are complex, and the s-channel unitarity cut produces the "pig tails" as shown in Fig. 5, which extend into nonphysical regions.

Also shown in Fig. 5 are the images of an s-channel bound-state pole, the t-channel unitarity cut, whose hadronic threshold is t_2, and a t-channel resonance.

The resulting IDR has the form

$$\mathrm{Re}A(t,a) = A^B_{\mathrm{IDR}}(t,a) + \frac{1}{\pi}\mathrm{P}\int_{\bar{t}}^{-\infty} \frac{\mathrm{Im}A^s(t',a)}{t'-t}dt' + \frac{1}{\pi}\mathrm{P}\int_{\bar{t}}^{0} \frac{\mathrm{Im}A^s(t',a)}{t'-t}dt' + \Delta_s(t,a) + \frac{1}{\pi}\mathrm{P}\int_{t_2}^{\infty} \frac{\mathrm{Im}A^t(t',a)}{t'-t}dt' , \quad \text{(A9)}$$

where $\bar{t} = t(\bar{s}(a), a)$, A^B_{IDR} is the bound-state pole contribution, and the superscripts s and t refer to the respective channel in which the physical amplitude is evaluated. Δ_s is the "pig tail" contribution, and represents the amplitude at unphysical values of t. For many reactions and for most interesting values of a (i.e., those for which the s-channel information in the first integral does not come from far forward scattering), $\bar{s}$ lies far below the occurrence of the first significant s-channel resonance, and the contribution of Δ_s can be expected to be small. Δ_s vanishes, of course, for $a = 0$.

The t-channel integral in Eq. (A9) is called the discrepancy function. It is determined by the t-channel background and singularities, and is expected to be smooth as a function of t in the s-channel physical and subthreshold regions. This smoothness assumption is vital to most IDR applications.

Further details on IDR can be found in Hite, Jacob, and Steiner.[1]

[1]G. E. Hite, Richard J. Jacob, and Frank Steiner, Phys. Rev. D 6, 3333 (1972).
[2]David C. Moir, Richard J. Jacob, and Gerald E. Hite, Nucl. Phys. B103, 477 (1976).
[3]Gerald E. Hite, Richard J. Jacob, and David C. Moir, Phys. Rev. D 12, 2677 (1975).
[4]G. E. Hite and R. J. Jacob, Phys. Lett. 53B, 200 (1974).
[5]Richard J. Jacob and Gerald E. Hite, Phys. Rev. D 11, 2466 (1975).
[6]F. Kaiser, E. Borie, and G. Höhler, Phys. Lett. 62B, 441 (1976); E. Borie and F. Kaiser, Nucl. Phys. B126, 173 (1977).
[7]Gerald E. Hite, Richard J. Jacob, and Michael D. Scadron, Phys. Rev. D 14, 1306 (1976). Referred to herein as HJS.
[8]G. E. Hite and R J. Jacob, Phys. Rev. D 5, 422 (1972); Nucl. Phys. B55, 587 (1973).
[9]S. Fubini and G. Furlan, Ann. Phys. (N.Y.) 48, 322 (1968).
[10]Stephen L. Adler, Ann. Phys. (N.Y.) 50, 189 (1968).
[11]Y. Nambu and E. Schrauner, Phys. Rev. 128, 862 (1962); Riazuddin and B. W. Lee, *ibid.* 146, B1202 (1966); G. Furlan, R. Jengo, and E. Remiddi, Nuovo Cimento 44, 427 (1966).
[12]E. Reya, Rev. Mod. Phys. 46, 545 (1974); see also Ref. 24, p. 48.
[13]This theorem is often referred to as the Adler consistency condition. S. L. Adler, Phys. Rev. 137, B1022 (1965).
[14]See, for example, Ref. 2.
[15]C. F. Chew, M. L. Goldberger, F. E. Low, and Y. Nambu, Phys. Rev. 106, 1345 (1957).
[16]J. S. Ball, Phys. Rev. 124, 2014 (1961).
[17]See S. B. Treiman, in S. B. Treiman, R. Jackiw, and D. J. Gross, *Lectures on Current Algebra and Its Applications* (Princeton Univ. Press, Princeton, 1972) pp. 38ff, for a discussion of this point.
[18]T. P. Cheng and R. Dashen, Phys. Rev. Lett. 26, 594 (1971); Phys. Rev. D 4, 1561 (1971).
[19]R. G. Moorhouse, H. Oberlack, and A. H. Rosenfeld, Phys. Rev. D 9, 1 (1974). Referred to herein as MOR
[20]F. A. Berends, A. Donnachie, and D. L. Weaver, Nucl. Phys. B4, 54 (1967). Referred to herein as BDW.
[21]Peter R. Weiler, Jr., Doctoral dissertation, Univ. of Wisconsin, 1971 (unpublished).
[22]For a discussion of contributions to discrepancy function uncertainties from s-channel integral errors, see Ref. 3; see also David Chandler Moir, Doctoral dissertation, Arizona State Univ., 1975 (unpublished).
[23]M. M. Nagels, *et al.*, Nucl. Phys. B109, 1 (1976).
[24]G. Furlan, N. Paver, and C. Verzegnassi, Nuovo Cimento A 62, 519 (1969). Referred to herein as FPV
[25]G. von Gehlen and M. G. Schmidt, Nucl. Phys. B20, 173 (1970). Referred to herein as GS.
[26]G. von Gehlen, Nucl. Phys. B20, 102 (1970).
[27]Steven L. Adler and Frederick J. Gilman, Phys. Rev. 152, 1460 (1966).
[28]P. Gensini, B. H. Kellett, N. Paver, and C. Verzegnassi, Phys. Lett. 53B, 197 (1974).
[29]A. Müllensiefen, Z. Phys. 211, 360 (1968).
[30]M. I. Adamovich, *et al.*, Sov. J. Nucl. Phys. 7, 360 (1970).
[31]P. Nölle, Diploma Thesis, Born, 1971 (unpublished).

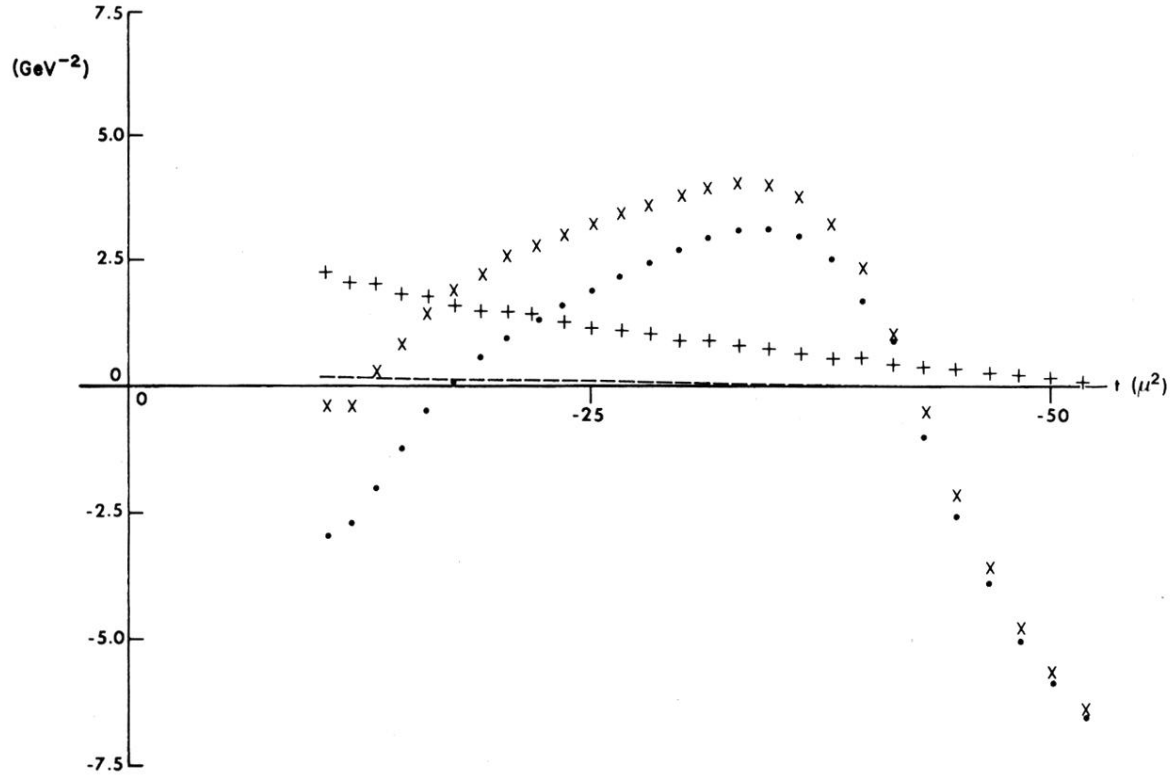

FIG. 1. s-channel physical-region contributions and discrepancy function for A_1^+. Dashed line indicates combined A_{IDR}^B and I_s^+, dotted line indicates I_s^-, xxx indicates $\mathrm{Re}A_1^+$, +++ indicates $D(t,0)$.

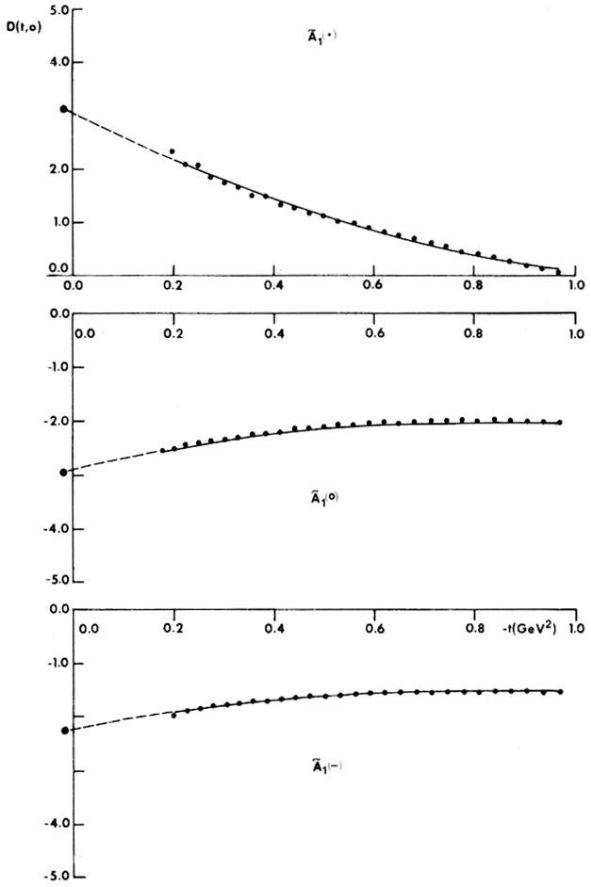

FIG. 2. Discrepancy functions for $\tilde{A}_1^i$, showing the best quadratic fit and extrapolation to $t=\mu^2$. Other extrapolations in this paper are to $t=-\mu^2$ (Breit threshold) and $t=-\mu^2(1-\mu/m_N)$ (physical threshold). $D(t,0)$ is shown in GeV units appropriate to the amplitudes (see Table I).

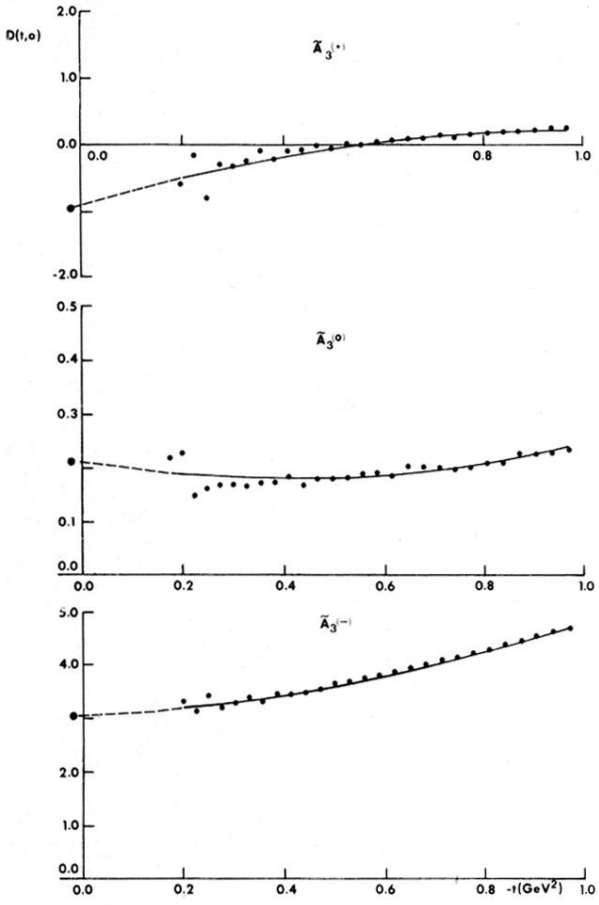

FIG. 3. Same as Fig. 2 for $\tilde{A}_3^i$. Large fluctuations near $t = -0.2$ GeV^2 in some amplitudes are due to large cancelations of imperfectly matched and rapidly varying real parts and "backward" integrals near the position of the $\Delta(1236)$ resonance.

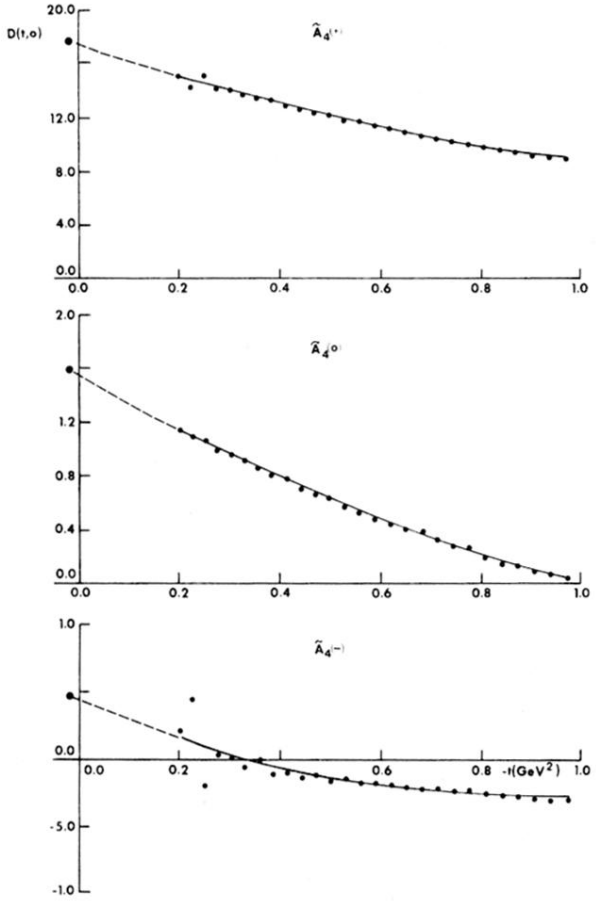

FIG. 4. Same as Figs. 2 and 3 for $\tilde{A}_4^{I}$.

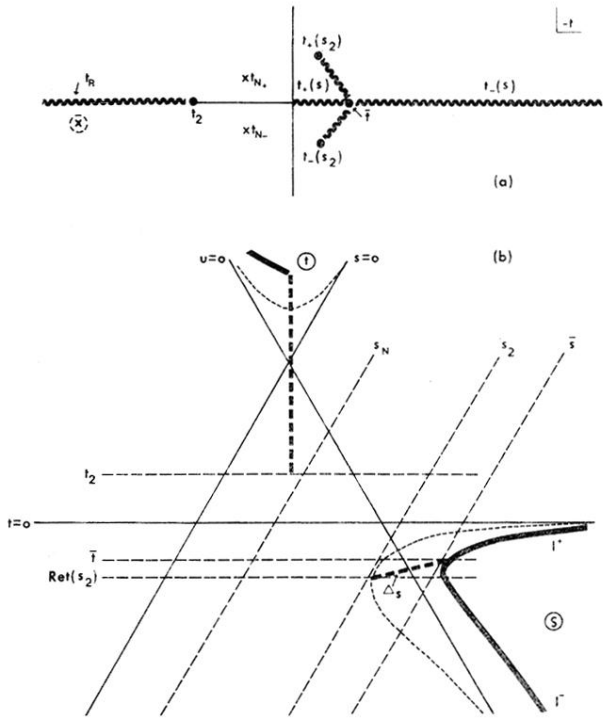

FIG. 5. Schematic representation of dynamical singularities for semielastic reactions. (a) shows the t channel, and images of the s channel, cuts and poles in the complex-t plane for fixed $a<0$. The "pig tails" leave the real t axis at $\bar{t}$ and progress to $t^{\pm}(s_2)$ as s approaches its threshold value, s_2. For $a=0$, $t^{\pm}(s_2)=\bar{t}$, and $t_{N+}=t_{N-}$ is also real. t_2 is the t-channel unitarity hadronic threshold, and t_R represents the position of a t-channel resonance on the second *dynamical* t sheet. The Mandelstam diagram (b) shows the location of these singularities with respect to the s- and t-channel physical regions. The u-channel unitarity cut appears on another *kinematical* t sheet, does not contribute to the dispersion relation, and is not pictured here. Physical-region boundaries are indicated by short-dashed lines and physical integration paths by heavy continuous lines. Heavy-dashed lines represent contributions to the dispersion relation from amplitudes at complex values of t, Δ_s being the contribution of the "pig tails" in (a). For $a=0$, $\Delta_s=0$, both heavy solid and dashed lines for $t>t_2$ contribute to the discrepancy function, $D(t,a)$.